Indian Journal of Geo Marine Sciences
Vol. 48 (05), May 2019, pp. 747-757

# Modelling a real rockslide as a static-dynamic transition using a material instability criterion

Z.H. Li[1], Y.J. Jiang[2*], Z.G. Tao[1], & M.C. He[1]

[1]State Key Laboratory for Geomechanics and Deep Underground Engineering, China University of Mining and Technology, Beijing, 100083, China

[2]Institute of Mountain Hazards & Environment, Chinese Academy of Sciences, Chengdu, China

*[E-mail: yuanjun.jiang.civil@gmail.com]

*Received 09 November 2017; revised 14 May 2018*

Failures at geological discontinuities often play a dominant role in the prediction of rockslides. In this study, a second order work criterion was used to analyze this type of problem by its constitutive instabilities, as it can expound all physical instabilities by divergence, except flutter instabilities. Derived from vanishing of the second order work, a matrix analysis focusing on the instability of geological discontinuities in two dimensions was performed. A real rockslide was simulated in a 2-D framework, and the second order work criterion was used to predict the occurrence of the rockslide. The numerical results were compared to monitoring data. Rockslides could be considered as processes involving a transition from a static loading to a dynamic response including a sudden burst of kinetic energy. Furthermore, a relationship existed between the second order work and second order kinetic energy. Hence, kinetic energy estimation was performed using two numerical approaches derived from this relationship and compared.

**[Keywords:** Rockslide; Geological discontinuity; Static-dynamic transition; Bifurcation instability; Kinetic energy; Second order work.]

## Introduction

A rock mass is a structural aggregation that consists of an intact rock block and geological discontinuities such as fractures, joints, and faults. The mechanical behaviors of these geological discontinuities frequently control the rock mass failure, because they are notably more degraded compared to that of an intact rock. In many real cases, the potential sliding surface of a rock slope is continually formed along a major geological discontinuity such as a fault or a weak zone. Thus, it is necessary to accurately analyze failure at geological discontinuities in stability problems of rock slopes. It can be considered that these geological discontinuities exhibit "soil-like" behaviors that can be described by elasto-plastic hardening models[1,2]. An incremental relationship between stress and strain is used to present the constitutive relation as follows:

$$d\boldsymbol{\sigma} = \boldsymbol{M} \cdot d\boldsymbol{\varepsilon} \quad \ldots (1)$$

where $d\boldsymbol{\sigma}$ and $d\boldsymbol{\varepsilon}$ are the incremental effective stress vector and incremental strain vector, respectively, and $\boldsymbol{M}$ is the elasto-plastic constitutive matrix.

As defined within the framework of classic plasticity theory, failure occurs when relative displacements along the geological discontinuity (or 'deformation' from a general view point) are sustained under a constant loading. Consequently, when the shearing stress reaches a peak, the corresponding shearing strain increases continuously under constant stresses. This can be considered as a failure that occurs in the geological discontinuity, and this will induce rockslides in a rock slope. Such analyses of failure lead to the notion of limit stress states corresponding to the plastic limit criterion such as the Mohr-Coulomb criterion. The limit analyses (conventionally termed as limit equilibrium methods) are widely used to analyze soil slopes or rock slopes that are heavily-fractured or weathered[7,9]. According to the definition of failure, this criterion corresponds to $\det(\boldsymbol{M}) = 0$, where $\det(\boldsymbol{M})$ is the determinant of the constitutive matrix $\boldsymbol{M}$.

However, results derived from the limit equilibrium methods are frequently unsatisfactory. Compared to the experimental results, the limit analysis presented by Adhikary and Dyskin[10] overestimated the failure level by at least 70%, but the stress-strain analysis results were more accurate with a maximum error of 15%. There are two reasons for this. The first reason

is the assumption that the plastic limit criterion was applicable throughout in accordance with the limit analysis; however, geomaterials in reality are effectively not homogeneous. The second reason is that geomaterials exhibit a rather non-associated behavior that induces the occurrence of failures before the plastic limit criterion. A bifurcation domain of failure existed in the stress space for geomaterials[2,6,11,14]. Rice's criterion could be reached prior to the plastic limit, in conjunction with the phenomena wherein increasing plastic deformation localizes in shear or compaction/dilation bands[15,17]. The second order work criterion could explain another bifurcation failure by excluding both the aforementioned criteria; diffuse failure that involves the liquefaction phenomenon of loose sand in an undrained condition is a typical example[11,14]. In this study, the second order work criterion was used to analyze failures of geological discontinuities,

$$d^2w = d\boldsymbol{\sigma} \cdot d\boldsymbol{\varepsilon} \quad \ldots (2)$$

where $d^2w$ denotes the second order work.

Second order work was initially described by Hill[18]; Darve et al. elucidated the bifurcation instabilities for geomaterials, established and validated the general framework of bifurcation failures theoretically, experimentally and numerically[11,14]. The second order work criterion is a new tool that is different from the plastic limit criterion and Rice's localization criterion. Additionally, it is the most conservative criterion as compared to the other two and can explain all types of material instabilities by divergence, except for flutter instabilities corresponding to abruptly cyclically increasing strains. The plastic limit criterion was included in the framework because the failure indicated by this criterion can be elucidated as a specific case. Furthermore, Rice's criterion involves a particular case in line with linear algebra[19,20], and thus localized failures could also be described within the framework.

## Materials and Methods

The paper discusses the second order work criterion that is applied to bifurcation instabilities of geological discontinuities. This is followed by the examination of the relationship between second order work and kinetic energy and the derivation of two approaches to estimate kinetic energy. Thereafter, the simulation of a real rockslide in China is examined. Real-time monitoring data were used and compared with the numerical results, and the kinetic energy was calculated and analyzed.

### *Second order work criterion applied to geological discontinuities and transition of static-dynamic regimes*

Hill's second order work theory was conveniently used to identify material instabilities by divergence, which resulted in failures[11,14]. Bursts of kinetic energy related to negative second order work further indicated effective failure[21,23]. As per the stress-strain analysis approach, the value of second order work stated in Equation (2) (that is, the necessary and sufficient conditions of failure) corresponded to three points: The current stress state, the loading direction, and appropriate loading manners[24]. A material is strictly stable if the calculated second order work is positive in every loading direction, and a material is potentially unstable if the calculated second order work is negative in any loading direction. Moreover, failure occurs if the second order work is negative in the current loading direction.

### *Bifurcation instabilities and second order work criterion in case of geological discontinuities*

The objective of this study involved analyzing material instability problems of geological discontinuities in two dimensions. Equation (2) can also be expressed as follows:

$$d^2w = d\tau \cdot d\gamma + d\sigma \cdot du \quad \ldots (3)$$

where $d\tau$ and $d\sigma$ are the tangential and normal incremental stress components, respectively (that are positive in compression). Correspondingly, $d\gamma$ and $du$ are the tangential and normal incremental strain components, respectively. Tensorial zones[25] in which the constitutive matrix $\boldsymbol{M}$ is constant were introduced to simplify the analysis. Equation (3) can be stated as follows:

$$d^2w = \begin{pmatrix} d\gamma \\ du \end{pmatrix}^T \boldsymbol{M} \begin{pmatrix} d\gamma \\ du \end{pmatrix} = \begin{pmatrix} d\gamma \\ du \end{pmatrix}^T \begin{pmatrix} G_t & G_n \\ E_t & E_n \end{pmatrix} \begin{pmatrix} d\gamma \\ du \end{pmatrix} \quad \ldots (4)$$

where $E_n$, and $G_t$ denote the normal and tangential stiffnesses, respectively; and $E_t$ and $G_n$ correspond to the dilatants feature of geological discontinuity. Hence, we obtain the following expression is obtained:

$$d^2w = E_n du^2 + (G_n + E_t) du d\gamma + G_t d\gamma^2 = d\gamma^2 \left( E_n \left( \frac{du}{d\gamma} \right)^2 + (G_n + E_t) \frac{du}{d\gamma} + G_t \right) \quad \ldots (5)$$

Let us consider that $d\gamma^2 > 0$ to study the conditions that resulted in $d^2w \leq 0$. This leads to the expression:

$$P(x) = E_n(X)^2 + (G_n + E_t)X + G_t \leq 0 \quad \ldots (6)$$

where $X = \frac{du}{d\gamma}$ denotes the loading direction. Evidently, $E_n$ represents a normal stiffness and is positive for most rocks ($E_n$ may be negative only in the case of compacting rocks with a high porosity[26]. Consequently, the conditions necessary to satisfy the inequality in Eq. (6) are expressed as:

$$\begin{cases} \Delta = (G_n + E_t)^2 - 4E_nG_t \geq 0 \\ \frac{du}{d\gamma} \in \left[\frac{-(G_n+E_t)-\sqrt{\Delta}}{2E_n}, \frac{-(G_n+E_t)+\sqrt{\Delta}}{2E_n}\right] \end{cases} \quad \ldots (7a, b)$$

Equation (7a) gives the condition of potential bifurcation instability. Equation (7b) indicates the loading directions leading to effective instability. According to Equation (7b), a series of cones existed in the bifurcation domain of the $(du, d\gamma)$ plane, based on tensorial zones in which a mechanical state situates (different tensorial zones correspond to different constitutive matrices). The loading directions along the two branches of the cones provided the exact nil value of second order work, and the directions inside the cones resulted in a negative value.

Furthermore, the second order work vanishes when the determinant of the symmetric part of the constitutive matrix, $\|\boldsymbol{M}^s\| = 0$, but not when $\|\boldsymbol{M}\| = 0$. Because geomaterials obey non-associated constitutive law, the corresponding constitutive matrix $\boldsymbol{M}$ was asymmetric, and its symmetric part can be written as:

$$\boldsymbol{M}^s = \begin{pmatrix} G_t & \frac{G_n+E_t}{2} \\ \frac{G_n+E_t}{2} & E_n \end{pmatrix} \quad \ldots (8)$$

The determinant of $\boldsymbol{M}^s$ is as follows:

$$\det(\boldsymbol{M}^s) = G_tE_n - \left(\frac{G_n+E_t}{2}\right)^2 = -\frac{\Delta}{4} \quad \ldots (9)$$

This was equivalent between$\Delta \geq 0$ and $\det(\boldsymbol{M}^s) \leq 0$. The plastic limit criterion corresponds to $\det(\boldsymbol{M}) = 0$ and is the upper limit of the bifurcation domain. The second order work criterion corresponding to $\det(\boldsymbol{M}^s) = 0$ is the lower limit. Linear algebra principles indicate that the determinant of the positive finite matrix exceeds that of its symmetric part[27], and this explains why the material instabilities by divergence can occur, from the mathematical viewpoint.

*Calculations of local and global second order works in boundary value problems*

In this study, the second order work was used in constitutive relations of geological discontinuities as a failure criterion, to investigate the instability of the rock slope and occurrence of rockslides from a constitutive viewpoint. Second order work was calculated only in the loading directions to ensure a reasonable computation time for the calculation; this could induce a smaller bifurcation domain because some other directions could potentially lead to instability earlier. This also involves the conservative assumption that a failure had occurred when the calculated second order work was not positive. In addition, to improve the readability of the corresponding graphs, $d^2w$ is normalized as:

$$d^2w^n = \frac{d^2w}{\|d\boldsymbol{\sigma}\|\|d\boldsymbol{\varepsilon}\|} \quad \ldots (10)$$

where $\|d\boldsymbol{\sigma}\|$ and $\|d\boldsymbol{\varepsilon}\|$ denote the norms of the stress increment vector and the strain increment vector, respectively. Hence, the value of $d^2w^n$ is limited between -1 and 1.

Moreover, a normalized global second order work criterion is used to apply the second order work to boundary value problems, and this is formulated as[6,28]:

$$D^2W = \frac{\Sigma(d^2w_i \cdot \omega_i J_i)}{\Sigma\,\omega_i J_i \Sigma(\|d\boldsymbol{\sigma}_i\|\|d\boldsymbol{\varepsilon}_i\|)} \quad \ldots (11)$$

where the subscript $i$ indicates the number of calculation points, $\omega_i$ and $J_i$ denote the numerical weight and the determinant of the Jacobian matrix at the point $i$, respectively. With respect to the numerical methods that did not involve the integration calculation, $\omega_i$ and $J_i$ were assigned the value of 1. According to equation (11), $D^2W \leq 0$ indicated global failure of the material.

*Transition between static-dynamic regimes*

The effective failure of geomaterials is associated with an outburst of kinetic energy[21,22] that declares the transition from a quasi-static regime to a dynamic regime. Let us consider the equation of motion:

$$\mathrm{div}\boldsymbol{\sigma} + \boldsymbol{b} = \rho\ddot{\boldsymbol{u}} \quad \ldots (12)$$

It was assumed that density $\rho$ is a constant and the time derivative of equation (12) is given by

multiplying the velocity vector $\dot{\boldsymbol{u}}$ on the left and right sides as a scalar product:

$$\left(\mathrm{div}\dot{\sigma} + \dot{b}\right) \cdot \dot{u} = \rho\ddot{u} \cdot \dot{u} \quad \ldots (13)$$

As $E_c = \frac{1}{2}\rho\|\dot{\boldsymbol{u}}^2\|$, we obtain$\ddot{E_c} = \rho\left\|\ddot{\boldsymbol{u}}^2\right\| + \rho\dot{\boldsymbol{u}}\dot{\ddot{\boldsymbol{u}}} = \rho(\dot{\boldsymbol{u}}\ddot{\boldsymbol{u}})$where $E_c$denotes kinetic energy. Consequently, Equation (13) can be written as:

$$\mathrm{div}(\dot{\boldsymbol{\sigma}} \cdot \dot{\boldsymbol{u}}) - \dot{\boldsymbol{\sigma}}\colon\dot{\boldsymbol{\varepsilon}} + \dot{\boldsymbol{b}} \cdot \dot{\boldsymbol{u}} = \ddot{E}_c - \rho\left\|\ddot{\boldsymbol{u}}^2\right\| \quad \ldots(14)$$

Thus, the relationship between second order work denoted as $d^2w/\Delta t^2 = \dot{\boldsymbol{\sigma}}\colon\dot{\boldsymbol{\varepsilon}}$ and kinetic energy as:

$$d^2w/\Delta t^2 = \mathrm{div}(\dot{\boldsymbol{\sigma}} \cdot \dot{\boldsymbol{u}}) + \dot{\boldsymbol{b}} \cdot \dot{\boldsymbol{u}} - \ddot{E}_c + \rho\left\|\ddot{\boldsymbol{u}}^2\right\| \quad \ldots (15)$$

The above equation proposed an approach to study the transition problems between the quasi-static regime in the pre-failure stage and the dynamic response at failures. In the framework, second order kinetic energy was linked with the external second order work involved with the external forces (the first and second terms), the internal second order work was related to the continuous constitutive behavior of the media, and finally the inertial term $\rho\left\|\ddot{\boldsymbol{u}}^2\right\|$ denoted the dynamic effect of the media, which remained positive and was close to zero under the quasi-static loading.

Equation (15) did not indicate a direct relationship between the second order work and kinetic energy. Indeed, a direct relation could be obtained by invoking Taylor's formula and the following initial conditions:

1) Assuming $\Delta t$sufficiently small and ignoring third order terms, $\frac{\ddot{E}_c(t)}{2!}\Delta t^2 \approx E_c(t+\Delta t) - E_c(t) - \dot{E}_c(t)\Delta t$
2) Considering that the media was in an equilibrium configuration at time $t$ and was unstable at time $t + \Delta t$, $E_c(t) = \dot{E}_c(t) = 0$

Thus, $\Delta t^2\ddot{E}_c(t) \approx 2E_c(t + \Delta t)$ and Equation (15) is expressed as follows:

$$d^2w(t)/\Delta t^2 \approx \mathrm{div}\left(\dot{\boldsymbol{\sigma}}(t) \cdot \dot{\boldsymbol{u}}(t)\right) + \dot{\boldsymbol{b}}(t) \cdot \dot{\boldsymbol{u}}(t) - 2E_c(t+\Delta t)/\Delta t^2 + \rho\left\|\ddot{\boldsymbol{u}}(t)^2\right\| \quad \ldots (16)$$

The first, second, and fourth terms on the right side of the above equation were close to zero because at the next moment when instability occurs, the increasing external loading cannot be applied and the inertial force remains a small value. This resulted in the following direct link as follows:

$$d^2w(t) \approx -2E_c(t + \Delta t) \quad \ldots (17)$$

According to this relationship, the increasing kinetic energy, which implies the instability evoking failure, induced a negative value of second order work. It was evident that Equation (17) was applicable only at the moment when failure occurred.

For estimating kinetic energy during quasi-static loading stage, two approaches could be derived. Let us introduce the assumption that $\Delta t$ was sufficiently small and take into account $\frac{\ddot{E}_c(t)}{2!}\Delta t^2 \approx E_c(t+\Delta t) - E_c(t) - \dot{E}_c(t)$, Equation (15) could be expressed for boundary value problems as follows:

$$E_c(t+\Delta t) \approx \frac{1}{2}\left(\int_{S_0} \dot{\boldsymbol{\sigma}} \cdot \dot{\boldsymbol{u}} \cdot \boldsymbol{n}dS_0 + \int_{V_0} \dot{\boldsymbol{b}} \cdot \dot{\boldsymbol{u}}\, dV_0 + \int_{V_0} \rho\left\|\ddot{\boldsymbol{u}}^2\right\| dV_0 - \int_{V_0} \dot{\boldsymbol{\sigma}} \cdot \dot{\boldsymbol{\varepsilon}} dV_0\right)\Delta t^2 + E_c(t) + \dot{E}_c(t)\Delta t = \frac{1}{2}(d^2W_{ext} - d^2W_{int} + I)\Delta t^2 + E_c(t) + \dot{E}_c(t)\Delta t \quad \ldots (18)$$

where $V_0$ denotes the volume of media subjected to body forces, and $S_0$ denotes the boundary of media subjected to surface forces. The kinetic energy of the media at the time step $t + \Delta t$ was calculated by the external second order work denoted by $d^2W_{ext} = \int_{S_0} \dot{\boldsymbol{\sigma}} \cdot \dot{\boldsymbol{u}} \cdot \boldsymbol{n}dS_0 + \int_{V_0} \dot{\boldsymbol{b}} \cdot \dot{\boldsymbol{u}}\, dV_0$, the inertial term denoted by $I = \int_{V_0} \rho\left\|\ddot{\boldsymbol{u}}^2\right\| dV_0$, the internal second order work denoted by $d^2W_{int} = \int_{V_0} \dot{\boldsymbol{\sigma}} \cdot \dot{\boldsymbol{\varepsilon}} dV_0$, the kinetic energy $E_c(t)$ and its differential $\dot{E}_c(t)$ at the time step *t*. This was the first approach to estimate the evolution of kinetic energy. With initial condition that $E_c(t_0) = \dot{E}_c(t_0) = 0, E_c(t + \Delta t)$ could be solved at each time step. It should be noted that this was an approximate approach and was thus limited to small time increments.

With respect to the second approach, Equation (15) could be expressed for boundary value problems as follows:

$$\ddot{E}_c = \int_{S_0} \dot{\boldsymbol{\sigma}} \cdot \dot{\boldsymbol{u}} \cdot \boldsymbol{n}dS_0 + \int_{V_0} \dot{\boldsymbol{b}} \cdot \dot{\boldsymbol{u}}\, dV_0 + \int_{V_0} \rho\|\ddot{\boldsymbol{u}}^2\|\, dV_0 - \int_{V_0} \dot{\boldsymbol{\sigma}} \cdot \dot{\boldsymbol{\varepsilon}} dV_0 \quad (19)$$

The second order kinetic energy of system was related to $d^2W_{ext}$, $I$, and $d^2W_{int}$, and thus an integration procedure with respect to time was required to calculate the kinetic energy. With the same initial condition as $E_c(t_0) = \dot{E}_c(t_0) = 0$, for each time $t_0 + \Delta t$, the integral expression from Equation (19) is expressed as:

$$E_c(t_0 + \Delta t) = \int_{t_0}^{t_0+\Delta t} \left( \int_{t_0}^{T} (d^2W_{ext} - d^2W_{int} + I) dt \right) dT \quad \ldots (20)$$

The concept of kinetic energy, failure, and second order work criterion could be used in many problems irrespective of the scale involved. In the following sections, these concepts are introduced with respect to macroscopic problems, such as the scale of rockslides, by means of numerical simulations.

*Simulation of a real rockslide*

In this study, the simulation was performed by means of FLAC-3D, which is a numerical tool based on the finite difference method. This numerical tool uses the full dynamic equations of motion even when modeling objects are static or quasi-static, and this characteristic made it possible to follow physically unstable processes without numerical complexities. In addition, an explicit solution scheme was selected to restrict the numerical cost. The small time limitation and the question of required damping posed delicate shortcomings for this type of formulation. However, they were overcome by automatic inertia scaling and automatic damping that did not influence the mode of failure.

A rock slope is considered as a rock mass separated by geological discontinuities. Accurately describing failures that occurred in the major geological discontinuity was the key point in investigating the occurrence of rockslides. As shown in Figure 1, the sliding bed is considered a stable and rigid block, and the sliding rock mass is considered one or several mobile and rigid blocks. Various factors such as earthquakes, rainfall, and charge loadings on top of the slope can induce sliding for a rockslide model of this type. However, with respect to a global viewpoint, the necessary and sufficient condition is that the sliding force induced from the upper blocks ($T_1$) should exceed the resistant force of the major geological discontinuity ($T_2$).

*Nanfen rockslide analyzed using second order work criterion*

The Nanfen open-pit mine is located in north-east China and is the largest single open pit iron mine in Asia. Up to now, more than 60 rockslides have occurred in this area, which has formed an old rockslide body of approximated 110000 $m^2$ and this pose a major threat to normal production. The landslide body contains mainly chlorite hornblende schist. A major fault with a $48^o$ inclination provides a potential principal sliding surface.

As shown in Figure 2, the monitoring points were distributed according to the structure and the scale of the old rockslide body in the foot-hanging wall in the mining site. Additionally, 28 monitoring points were installed to measure the sliding force (blue round dots) in the sliding body (334-662 m bench). A GPRS relay station, a Beidou satellite relay station, and a rain-fall monitoring point were installed in the hanging wall that was stable as compared to the foot hanging wall.

The sliding force could be derived from the monitored data with a remote real-time monitoring system developed by He[29,31]. Figure 3 shows the evolution of the sliding force along the geological discontinuity from B334 to B358 (see Fig. 2), which

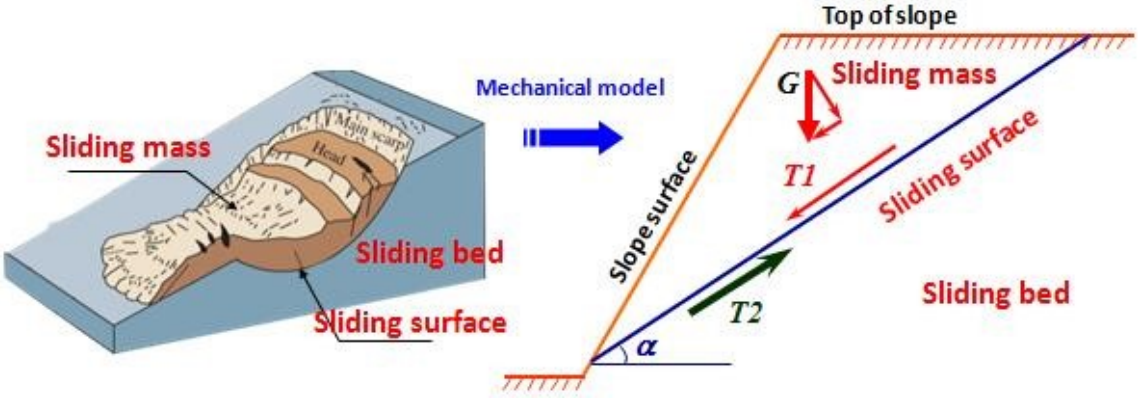


Fig. 1 — Mechanical model for rock slopes controlled by one major geological discontinuity

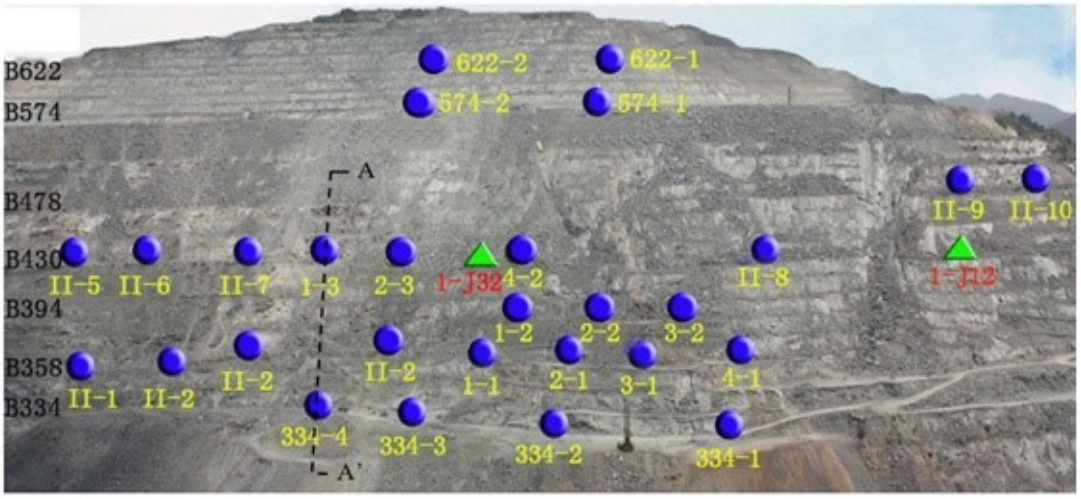


Fig. 2 — Distribution of monitoring points

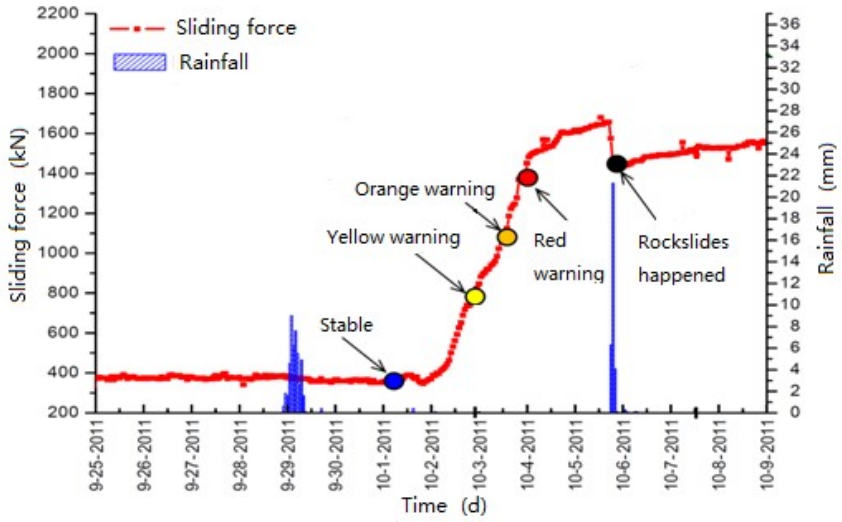


Fig. 3 — Monitoring sliding force against time[29]

was principally induced by mining activities at the toe of the slope. The effect of rainfall was not considered because it had not rained in the transition process from a stable state to rockslide as shown in Figure 3 (Noted that rainfalls occurred on September 29, 2011 and particularly on October 6, 2011 could trigger a saturation process in the major fault and introduce a potential factor of instability). The sliding force remained stable until August 2, 2011, and increased rapidly to 1678 kN on October 6, 2011, when the rockslide occurred[29].

First, it was reasonable to consider this real case by using the mechanical model illustrated in Figure 1 because the real rock slope presented an obvious mechanical discontinuity according to the geological data in Table 1, and it was the failure of the major fault that induced the rockslide. Second, this case could be analyzed using Equations (3-9) because the failure of the major fault occurred under an increasing sliding force and a constant normal force. In the framework of a 2-D analysis, the loading conditions corresponded to $d\sigma = 0$ and $d\tau > 0$. According to Equations (3-5) and $d\sigma = E_t d\gamma + E_n du = 0$, the second order work under this loading path is expressed as:

$$d^2w = d\tau \cdot d\gamma = d\gamma^2 \left(G_n \frac{du}{d\gamma} + G_t\right) = d\gamma^2 \left(-G_n \frac{E_t}{E_n} + Gt \leq 0\right) \quad \ldots (21)$$

Table 1 — Physical parameters for rock mass and fault of Nanfen rockslide[32]

| Physical parameters | $E$ | $v$ | $c$ | $\varphi$ | $\psi$ | $\rho$ |
|---|---|---|---|---|---|---|
| Unit | MPa | - | kPa | ° | ° | Kg/m³ |
| Rock mass | 36000 | 0.31 | 317 | 37 | 8 | 2910 |
| Fault | 800 | 0.26 | 12 | 24.7 | 2 | 1825 |

It was assumed that $d\gamma^2 \geq 0$, and thus the condition of $d^2w \leq 0$ is

$$\frac{E_t}{E_n} \geq \frac{G_t}{G_n} \quad \ldots (22)$$

Evidently, this condition was equivalent to $\det(\boldsymbol{M}) \leq 0$, which corresponded to the plastic limit criterion. Consequently, under this loading path, the failure occured exactly at the plastic limit criterion and bifurcation instability did not exist prior to the same. However, Equation (22) was always included in $\Delta = (G_n + E_t)^2 - 4E_nG_t \geq 0$, and this is another example wherein the second order work criterion included the plastic limit criterion. It should be noted that failures of major faults occurring during rainfalls involved a decreasing $\sigma$. If rainfall was sufficiently intense and the permeability of the major fault was sufficiently low, an undrained condition could lead to bifurcation instabilities before the plastic limit. This is why the second order work criterion was recommended to analyze the instability problems of the rock slope.

*Numerical model of Nanfen rockslide*

As shown in Figure 4, the slope has a major fault with an inclination of 48°, a height of 36 m, and a thickness of 3 m. The monitored sliding force was assumed as a shearing stress that increased linearly from the top of the slope to the toe and was incident along the upper surface of the fault. During the calculation, the shearing stress was increased until global failure (loss of convergence) occurred. It should be noted that the upper block was neglected because the calculation was only performed with respect to the major fault. The effects of the upper block on the major fault were considered to have been caused initially by gravity (initialization of gravity caused an initial sliding force of 380 kN) and then by the shearing force.

The strain hardening Mohr-Coulomb model was selected according to the physical parameters in Table 1 and the second order work was implanted in FLAC as the failure criterion. In this study, we did not repeat details of this model, but only recalled

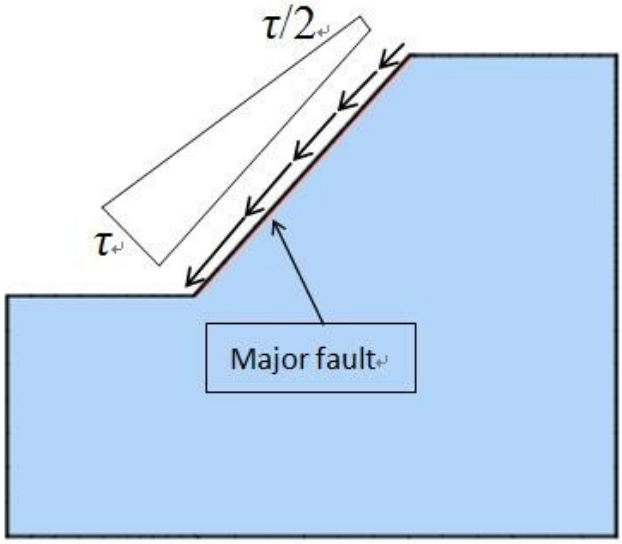


Fig. 4 — Rockslide model in 2D

the corresponding yield surface and the potential function, written as:

$$\begin{cases} f = \sigma_1 - \sigma_3 N_\varphi - 2c\sqrt{N_\varphi} \\ g = \sigma_1 - \sigma_3 N_\psi \\ N_\varphi = \frac{1+\sin\varphi}{1-\sin\varphi} \\ N_\psi = \frac{1+\sin\psi}{1-\sin\psi} \end{cases} \quad \ldots (23)$$

where $\varphi$ and $c$ denote the effective angle of friction and cohesion, respectively. Furthermore, $\psi$ denotes the dilation angle. Moreover, $f \neq g$, and thus this was a non-associated constitutive model, and the corresponding constitutive matrix was not symmetric.

**Results and Analysis**

The rockslide was induced by failure at the major fault, and the evolution of second order work in the major fault was proposed to highlight this point. Three points in the major fault were selected to present the local second order work curves in Figure 5. Evidently, the local second order works at the toe of slope and in the middle (points A and B) decreased and vanished at load step 20. This implied that some zones in the lower part of the major fault

became unstable at load step 20 under a sliding force of 1453.3 kN. In contrast, the local second order work near the top of the slope (point C) remained positive during the calculations.

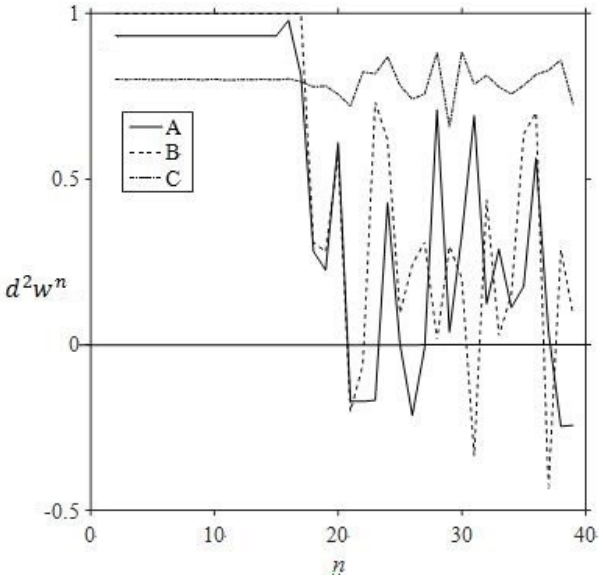


Fig. 5 — Evolution of local $d^2w^n$ at three points in major fault

Figures 6a-e show the contours of local second order work along the major fault that globally coincided with the result in Figure 5. Given a shearing force of 1467.8 kN, first unstable zones appeared and were evidently distributed in the toe and the middle of the fault in Figure 6a. It is important to note that a red warning was actually issued as shown in Figure 3 to stop excavation activity at the toe of the slope. With respect to the increasing sliding force (as illustrated in Figs 6b-d under sliding forces of 1526, 1656.7, and 1714.9 kN), the unstable zones as indicated by the second order work criterion extended progressively near the top of the slope. When the sliding force reached 1729.4 kN (as shown in Fig. 6e), a through failure appeared along the major fault and the sliding body moved. The results in gross terms of the maximum sliding force predicted by this numerical approach coincided with those of the real case shown in Figure 3.

The global second order work began decreasing from step 15 and was negative at load step 39 (see Fig. 7). With respect to load step 39, the sliding force was 1729.4 kN and a through instability zone

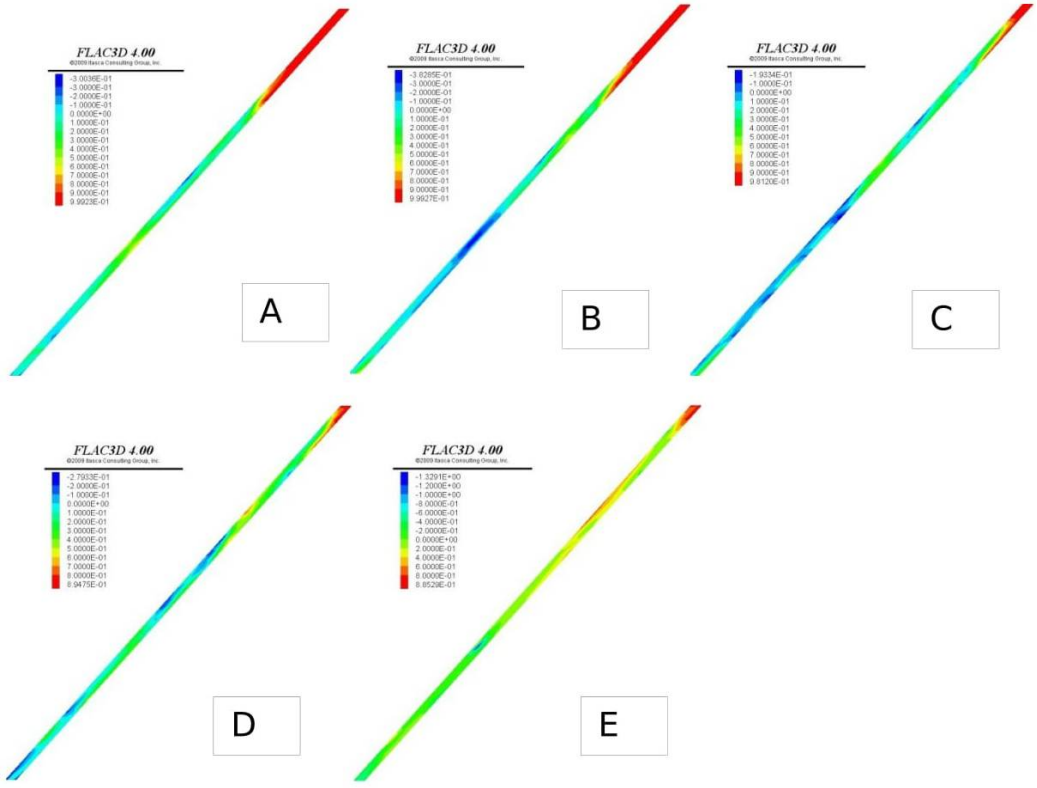


Fig. 6a — Contour of local $d^2w^n$ under sliding force of 1467.8kN at load step 21; 6b — Contour of local $d^2w^n$ under sliding force of 1526kN at load step 25; 6c — Contour of local $d^2w^n$ under sliding force of 1656.7kN at load step 34; 6d — Contour of local $d^2w^n$ under sliding force of 1714.9kN at load step 38; 6e — Contour of local $d^2w^n$ under sliding force of 1729.4kN at load step 39

appeared (as shown in Fig. 6e). This result coincided with the evolution of a maximum unbalance force as shown in Figure 8. This force was related to the inertial force and remained at a sufficiently small value to ensure the balance of the system forces. As shown in Figure 8, the force slowly increased and a small peak appeared after loading step 20 due to the first instability zones in the lower part of the major fault. Furthermore, the first abrupt decrease in global second order work also occurred. With respect to the real case, a red warning was issued under the corresponding sliding force (as shown in Fig. 3). The force increased sharply with respect to the shearing loading before load step 39, and this indicated a sudden kinetic energy burst in the major fault, which evoked a global failure and a dynamic response.

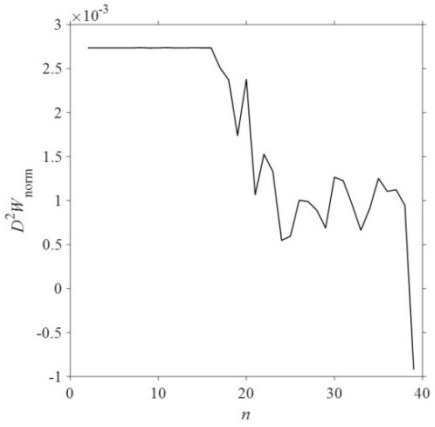


Fig. 7 — Evolution of normalized global second order work in the major fault

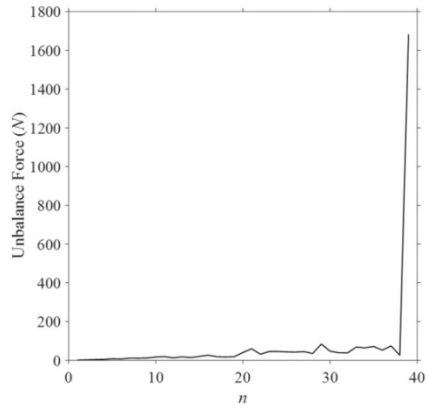


Fig. 8 — Evolution of maximum unbalance force

The kinetic energy of the major fault was estimated according to Equations (18 and 20) as shown in Figure 9a, and two zooms to a smaller load step and a load step closed to the failure were demonstrated in Figure 9b and c. The studied media remained at a low kinetic energy during the quasi-static loading, and the energy increased more quickly after load step 20, wherein a local instability appeared. An energy burst appeared at load step 39, which indicated the occurrence of the global failure and the transfer of media into dynamic regime. The approximation approach could not show the energy burst at failure because Toylar's formula was an appropriate tool for smooth function, and the energy function was no longer continuous at failure, this was why estimations of the two approaches remained a good coincidence in the quasi-static loading stage, but the case changed when failure occurred. Additionally, energy calculated from Equation (18) was less than that from integration approach in case that the media remained a very small energy, and the case was contrary when energy of the media was large.

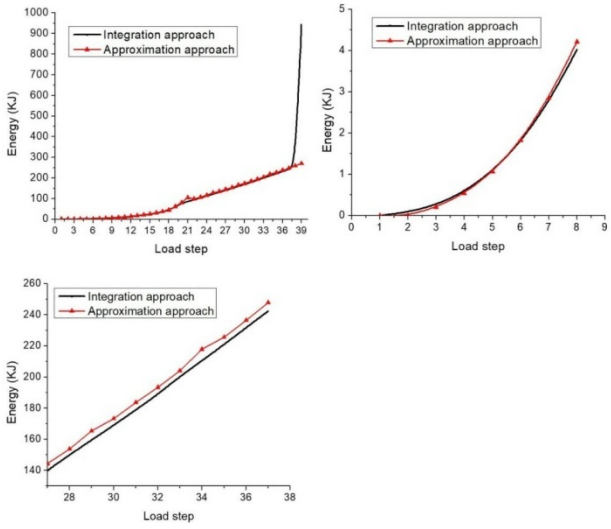


Fig. 9a-c — Kinetic energy estimated according to Equations (18 and 20)

Finally, it is important to note that, although the kinetic energy estimation is just a heuristic attempt, the result is qualitatively acceptable. Hence, it is worthwhile to explore a large scale approach that assesses the kinetic energy of a geological disaster.

## Conclusion

The study involved the analysis and simulation of a real rockslide as a static-dynamic transition in the bifurcation instability framework. First, an analysis using the second order work criterion was performed for the rock slopes controlled by a major discontinuity. With respect to the real landslide simulated in the study, the stress-strain analysis indicated that bifurcation failure would not occur under certain loading paths. However, second order work continued to be an appropriate tool because it includes all bifurcation failures by divergence, including the plastic limit criterion and excluding flutter instability. Second, according to the numerical results of the real landslide, an approximated peak of the sliding force was obtained and compared to the monitoring data. Additionally, a through instability zone was presented under this sliding force peak. Third, global second order work was introduced to predict the occurrence of the rockslide, and the kinetic energy derived from the second order work was estimated to describe the static-dynamic regime transition. The corresponding results coincided with the evolution of the maximum unbalance force calculated by FLAC, and the kinetic energy results estimated from two numerical approaches were qualitatively satisfactory and shed light on the discontinuity of energy evolution when failure occurred. A quantitative validation could be performed later and will provide an expected approach to estimate the kinetic energy of rockslides in addition to detailing important suggestions for engineering.

In conclusion, the second order work criterion could accurately predict the failure of geological discontinuities in addition to those of soils. The stress-strain analysis approach based on this could be considered as reliable in analyzing and predicting rockslides induced by major geological discontinuity failures. In consideration of its capacity to describe all physical bifurcation instabilities (excluding flutter instability) and the relation between failure and energy burst, the second order work criterion can be recommended.

## Acknowledgement

This work was supported by the CAS Pioneer Hundred Talents Program and the Major Program of National Natural Science of Foundation of China (41502334).

## References

1 Duriez, J., Darve, F., & Donze, F.V. (2011). Incrementally non-linear plasticity applied to rock joint modelling. *International Journal for Numerical and Analytical Methods in Geomechanics, 37(5), 453-477.*

2 Merrien-Soukatchoff, V., Duriez, J., Gasc, M., Darve, F., & Donze, F.V. (2011). Mechanical stability analyses of fractured rock slopes. In *Rock Engineering, Lambert S, Nicot F(eds). John Wiley & Sons/ISTE Ltd: New York/London.*

3 Lignon, S., Laouafa, F., Prunier, F., Khoa, H. D. V., & Darve, F. (2009). Hydro-mechanical modelling of landslides with a material instability criterion. *Géotechnique, 59(6), 513-524.*

4 Prime, N., Dufour, F., & Darve, F. (2014). Solid-fluid transition modeling in geomaterials and application to a mud flow interacting with an obstacle. *International Journal for Numerical and Analytical Methods in Geomechanics, 38, 1341-1361.*

5 Li, Z.H. (2015). Modéisation des glissements de terrain dans le cadre hydromécanique. *Ph.D. Thesis, Université Grenoble Alpes.*

6 Li, Z.H., Dufour, F., & Darve, F. (2018). Modelling rainfall-induced mudflows using FEMLIP and a unified hydro-elasto-plastic model with solid-fluid transition. *European Journal of Environmental and Civil Engineering, 22(4):491-521.*

7 Livesley, R. (1978). Limit analysis of structures formed from rigid blocks. *International Journal for Numerical Methods in Engineering, 12, 1853-1871.*

8 Aydan, O., Kawamoto, T. (1992). Stability of slopes and underground openings against flexural toppling and their stabilization. *Rock Mechanics and Rock Engineering. 25(3), 143-165.*

9 Durand, A., Vargas, E. Jr., & Vaz, L. (2006). Application of numerical limit analysis (NLA) to stability problems of rock and soil masses. *International Journal of Rock Mechanics and Mining Sciences, 43, 408-425.*

10 Adhikary, D.P., Dyskin, A.V. (2007). Modelling of progressive and instantaneous failures of foliated rock slopes. *Rock Mechanics and Rock Engineering, 40(4), 349-362.*

11 Darve, F., Servant, G., Laouafa, F., & Khoa, H.D.V. (2004). Failure in geomaterials : continuous and discrete analyses. *Computer Methods in Applied Mechanics and Engineering, 193(27-29), 3057-3085.*

12 Khoa, H.D.V., Georgopoulos, I.O., Darve, F., & Laouafa, F. (2006). Diffuse failure in geomaterials. *Computers and Geotechnics,33, 1-14.*

13 Laouafa, F., Prunier, F., Daouadji, A., Al Gali, H., & Darve, F. (2011). Stability in geomaterials, experimental and numerical analyses. *International Journal for Numerical and Analytical Methods in Geomechanics, 35, 112-139.*

14 Prunier, F., Laouafa, F., Lignon, S., & Darve, F. (2009). Bifurcation modelling in geomaterial : From the second-order work criterion to spectral analyses. *International Journal for Numerical and Analytical Methods in Geomechanics, 33, 1169-1202.*

15 Rudnicki, J.W., Rice, J. (1975). Conditions for the localization of deformation in pressure sensitive dilatants materials. *International Journal of Solids and Structures, 23, 371-394.*

16 Rice, J. (1976). The localization of plastic deformation. *Delft IUTAM Proceedings, Koiter ed., 1, 207-220.*

17 Daouadji, A., Jrad, M., Prunier, F., Sibille, L., Nicot, F., Laouafa, F., & Darve, F. (2012). Divergence instability and diffuse failure in granular media. *Procedia IUTAM, 3, 115-140.*

18 Hill, A. (1958). A general theory of uniqueness and stability in elastic-plastic solids. *Journal of the Mechanics and Physics of Solids, 6, 236-249.*

19 Bigoni, D., Hueckel, T. (1991). Uniqueness and localization-I, Associative and non-associative elastoplasticity. *International Journal of Solids and Structures, 28(2), 197-213.*

20 Nicot, F., Darve, F. (2011). Diffuse and localized failure modes: Two competing mechanisms.*International Journal for Numerical and Analytical Methods in Geomechanics, 35(5), 586-601.*

21 Nicot, F., Sibille, L., & Darve, F. (2012). Failure in rate-independent granular materials as a bifurcation toward a dynamic regime. *International Journal of Plasticity,29, 136-154.*

22 Nicot, F., Daouadji, A., Laouafa, F., & Darve, F. (2011). Second-order work, kinetic energy and diffuse failure in granular materials. *Granular Matter,13(1), 19-28.*

23 Nicot, F., Daouadji, A., Laouafa, F., & Darve, F. (2011). Second-order work, kinetic energy and diffuse failure in granular materials. *Granular Matter,13(1), 19-28.*

24 Daouadji, A., Darve, F., Gali, H.A., Hicher, P.Y., Laouafa, F., Lignon, S., Nicot, F., Nova, R., Pinheiro, M., Prunier, F., Sibille, L., & Wan, R. (2011). Diffuse failure in geomaterials: experiments, theory and modeling. *International Journal for Numerical and Analytical Methods in Geomechanics, 35(16), 1731-1773.*

25 Darve, F., Servant, G. (2004). Fundamental of constitutive equations for geomaterials. *Degradations and instabilities in geomaterials.*

26 Mollema, P., Antonellini, M. (1996). Compaction bands: a structural analog for anti-mode I cracks in aeolian sandstone. *Tectonophysics, 267(1-4), 209-228.*

27 Ostrowski, A.M., Taussky, O. (1951). On the variation of the determinant of a positive finite matrix 1. *Indagationes Mathematicae, 54(2), 383-385.*

28 Li, Z.H., Dufour, F., & Darve, F. (2016). Hydro-elasto-plastic modelling with a solid/fluid transition. *Computers and Geotechnics, 75, 69-79.*

29 Tao, Z.G., Li, H.P., Sun, G.L., Yin, L.J., & Zhang, X.L. (2015). Development and application of monitoring system for landslides on the basis of rock anchor with a negative Poisson's ratio (in Chinese). *Rock and Soil Mechanics, 36(10), 3032-3039.*

30 He, M.C. (2009). Real-time remote monitoring and foresting system for geological disasters of landslides and its engineering application. *Chinese Journal of Rock Mechanics and Engineering, 28(6), 1081-1090.*

31 He, M.C., Gong, W.L., Wang, J., Qi, P., Tao, Z.G., Du, S., & Peng, Y.Y. (2014). Development of a novel energy-absorbing bolt with extraordinarily large elongation and constant resistance. *International Journal of Rock Mechanics and Mining Sciences, 67, 29-42.*

32 Sun, D.X., Tao, Z.G., Fan, L.J., & Feng, X.R. (2011). Stability assessment and sensibility analysis of Nanfen open-pit mine slope (in Chinese). *Metal Mine, 5, 57-60.*